Charge transport in hybrid halide perovskites

Mingliang Zhang, Xu Zhang, Ling-Yi Huang, Hai-Qing Lin, and Gang Lu

Phys. Rev. B **96**, 195203 — Published 7 November 2017

DOI: 10.1103/PhysRevB.96.195203

Charge Transport in Hybrid Halide Perovskites

Mingliang Zhang[1,2], Xu Zhang[2], Ling-Yi Huang[2], Hai-Qing Lin[1†] and Gang Lu[2*]
[1] *Beijing Computational Science Research Center, Beijing 100193, China and*
[2] *Department of Physics and Astronomy, California State University Northridge, Northridge, CA 91330, USA*

Charge transport is crucial to the performance of hybrid halide perovskite solar cells. A theoretical model based on large polarons is proposed to elucidate charge transport properties in the perovskites. Critical new physical insights are incorporated into the model, including the recognitions that acoustic phonons as opposed to optical phonons are responsible for the scattering of the polarons; these acoustic phonons are fully excited due to the "softness" of the perovskites, and the temperature-dependent dielectric function underlies the temperature dependence of charge carrier mobility. This work resolves key controversies in literature and forms a starting point for more rigorous first-principles predictions of charge transport.

PACS numbers: 72.10.Di, 72.10.Fk, 72.40.+w, 72.20.Jv

I. INTRODUCTION

Organic-inorganic hybrid perovskites represent a fascinating class of materials poised to revolutionize optoelectronic, in particular, photovoltaic applications[1–3]. These materials possess a set of unusual transport properties crucial to their photovoltaic performance. Essential to the transport properties is charge carrier mobility μ, which exhibits following behavior unique to this family of materials: (1)$\mu \propto n^{-1}$ where n is charge carrier concentration[4]; (2)$\mu \propto I_0^{-1/2}$ where I_0 is incident photon flux[5]; (3)$\mu \propto T^{-3/2}$ where T is temperature[5–9]; and (4)μ is insensitive to defects[10,11]. There is great interest to understand and control the transport properties of the perovskites, further propelling the development of perovskite-based solar cells. However, no complete physical picture has emerged so far to fully account for the experimental observations on charge transport and the nature of charge transport remains a subject of intense debate[10–13].

In this paper, we propose a theoretical model to elucidate the charge transport behavior in the perovskites. In this model, the charge carriers are characterized as large polarons, resulted from the carrier interaction with optical phonons[10]. Hence the residual interaction between the polarons and the optical phonons is much weaker than the interaction with acoustic phonons. The charge transport is determined by the scattering of the polarons by themselves, defects and longitudinal acoustic (LA) phonons and is governed by Boltzmann equation. These interactions are screened by a temperature-dependent dielectric function as a result of spontaneous polarization in the perovskites at low temperatures. Owing to the "softness" of the perovskites, the LA phonons are fully excited, interacting strongly with the polarons. The constant carrier concentration n leads to an equilibrium distribution function of the polarons that is proportional to n, resulting in n-dependent carrier mobilities.

II. NATURE OF CHARGE CARRIERS

In the following, we take $MAPbI_3$ [MA^+=$(CH_3NH_3)^+$] as a representative of ABX_3 perovskite family to illustrate the general physical picture of charge transport.

A. Properties of of large polarons

In $MAPbI_3$, the interaction between a free carrier and longitudinal optical (LO) phonons (i.e., Pb-I stretching modes) is stronger than that between the carrier and the acoustic phonons[14], supported by the emission line broadening experiment[12]. According to the theory of large polarons[15], the binding energy, radius and effective mass of a large polaron can be expressed as $E_{\rm P} = V_L^2/4T_e$, $R_{\rm P} = 2T_e a/V_L$, and $m_{\rm P} = V_L^4[4\omega_{\rm LO}^2 a^2 T_e^3]^{-1}$, respectively. Here $\omega_{\rm LO}$ is the frequency of the LO phonon and a is the lattice constant of $MAPbI_3$; $T_e \sim \hbar^2/(2mr^2)$ is the kinetic energy of the conduction electrons, where m is the mass of the electron, r is the characteristic length-scale over which the wave-function of the conduction electron changes substantially, taken as the mean value between the radius of Pb^{2+} ion and Pb atom[16,17], i.e., r ∼1.675 Å. V_L represents the interaction between the carrier and the LO phonon-induced electric field,

$$V_L \sim \frac{1}{4\pi\epsilon_0}\frac{e^2}{2}\left(\frac{1}{\varepsilon_\infty} - \frac{1}{\varepsilon_0}\right)\frac{1}{r}, \tag{1}$$

where ε_0 and ε_∞ are static and optical dielectric constant. Using both experimentally measured[18,19] and first-principles computed[20,21] parameters of $MAPbI_3$, we estimate $E_{\rm P}$ ∼ 67 - 112 meV, $R_{\rm P}$ ∼ 22 - 28 Å and $m_{\rm P}$ ∼ 4.1 − 12 m. Since $E_{\rm P}$ is much higher than the room temperature, these polarons are thermally stable, in line with the large polaron hypothesis for charge transport[10,11,13,20,22–24]. We can also estimate the critical concentration of the polarons as $n_c = (2R_{\rm P})^{-3} \sim 5.5 \times 10^{18}{\rm cm}^{-3}$; beyond this critical value, neighboring polarons would overlap. In normal operating conditions of the solar cells, the free carrier concentration n is [6,9]

less than 10^{18}cm^{-3} and n_c, thus the large polarons could avoid each other in $MAPbI_3$.

B. Distribution function of polarons

The Fermi-Dirac distribution of polarons can be approximated by the Boltzmann distribution[25] if

$$(\frac{2\pi\hbar^2}{m_{\rm P}k_BT})^{3/2}n \ll 1. \quad (2)$$

Under the normal operating conditions, this equation is satisfied, thus the photo-generated electrons are non-degenerate and one can replace the Fermi-Dirac distribution by the Boltzmann distribution. Later we will show that the polaron state can be characterized by its momentum $\mathbf{p}$, and the energy of the polaron state $|\mathbf{p}\rangle$ is thus denoted as $\varepsilon_{\mathbf{p}}$.

In an intrinsic or lightly doped $MAPbI_3$, the carriers are generated primarily by photo- as opposed to thermal excitations. Thus n is determined by I_0, and largely independent[5,26] of T. Hence, we can express the occupation number $f_0(\varepsilon_{\mathbf{p}})$ per spin for polarons of energy $\varepsilon_{\mathbf{p}}$ as:

$$f_0(\varepsilon_{\mathbf{p}}) = \frac{4\pi^{3/2}\hbar^3 e^{-\varepsilon_{\mathbf{p}}/k_BT}}{(2m_{\rm P}k_BT)^{3/2}}n. \quad (3)$$

As will be shown later, the linear n dependence of the polaron distribution function gives rise to the n dependence of carrier mobility.

C. Formation free energy of polarons

To further establish the fact that the polarons are thermodynamically stable than free electrons in $MAPbI_3$ under the normal operating conditions, we next estimate the formation *free* energy of the polarons relative to that of the free electrons. There are two major contributions to the entropy of the polarons. Once a polaron is formed, it acquires an excluded volume and increases its effective mass, leading to higher translational entropy. At the same time, the induced lattice distortion due to the polaron increases the vibrational frequencies and lowers the vibrational entropy. In the following, we will estimate these competing contributions to the entropy.

1. *Change in translational entropy*

It is known that the translational entropy for non-degenerate free electron gas of N electrons occupying a volume of V, is

$$S_{\rm g} = Nk_B[\ln\frac{V}{N}(\frac{2\pi mk_BT}{h^2})^{3/2} + \frac{5}{2}], \quad (4)$$

where h is the Planck constant.[27]

If all electrons become polarons, the free volume V_f for the polarons is reduced to $V_f = V - N4\pi R_{\rm P}^3/3$, and their corresponding translational entropy $S_{\rm P}$ becomes[27]

$$S_{\rm P} = Nk_B[\ln\frac{V_f}{N}(\frac{2\pi m_{\rm P}k_BT}{h^2})^{3/2} + \frac{5}{2}], \quad (5)$$

where $m_{\rm P}$ is the polaron mass. Thus, the change in entropy Δs_e per electron is

$$\Delta s_e = (S_{\rm P} - S_{\rm g})/N = k_B\ln(1 - n\frac{4\pi R_{\rm P}^3}{3})(\frac{m_{\rm P}}{m})^{3/2}, \quad (6)$$

where $n = N/V$ is the number of free electrons per unit volume. From Eq. (6), one can see that (i) Δs_e does not depend on temperature; (ii) the larger the $m_{\rm P}$, the higher the entropy; (iii) the finite size of the polarons decreases their entropy relative to the electrons. Under the normal conditions, the concentration n of the polarons is much less than n_c, therefore the translational entropy of the polarons is higher than that of the free electrons, i.e., $\Delta s_e > 0$.

2. *Change in vibrational entropy*

The entropy S_1 of a harmonic oscillator with frequency ω is given by[25]:

$$S_1 = -k_B\ln(1 - e^{-\hbar\omega/k_BT}) + \frac{\hbar\omega}{T}\frac{e^{-\hbar\omega/k_BT}}{1 - e^{-\hbar\omega/k_BT}}. \quad (7)$$

In a undeformed crystal, the entropy S_{10} due to a single LO mode can be obtained from Eq. (7) by letting $\omega = \omega_{\rm LO}$, where $\omega_{\rm LO}$ is the frequency of the LO mode. In each primitive cell of $MAPbI_3$, the vibrational frequencies of three stretching modes (Pb-I bonds) are increased due to the lattice distortion. Hence, the vibrational entropy is decreased.

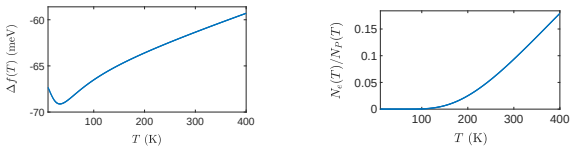

(a) (b)

FIG. 1. (a) Formation free energy as function of temperature; (b) The ratio of number of electrons (N_e) to the number of polarons (N_P) vs. temperature.

Comparing to free electrons in a undeformed lattice, the change in the vibrational entropy Δs_v per polaron is:

$$\Delta s_v = -3\frac{\frac{4}{3}\pi R_{\rm P}^3}{a^3}(S_1 - S_{10}), \quad (8)$$

where $\frac{4}{3}\pi R_{\rm P}^3/a^3$ accounts for the number of the primitive cells occupied by a large polaron, and the factor of 3 represents the three Pb-I stretching modes. If temperature is higher than 50 K, the decrease of the vibrational entropy dominates the change in the translational entropy, cf. Fig.1(a).

3. Relative contributions to conductivity from polarons and electrons

The change in entropy Δs in forming a polaron is

$$\Delta s = \Delta s_e + \Delta s_v. \tag{9}$$

The formation free energy Δf per polaron is thus

$$\Delta f(T) = -E_{\rm P} - T\Delta s, \tag{10}$$

which is plotted as a function of temperature in Fig.1(a). The shallow minimum in Fig.1(a) is due to the larger effective mass $m_{\rm P}$ of polarons and $n \ll n_c$. With the increase of temperature, $|\Delta f(T)|$ is decreased, i.e., polarons become less stable at a higher temperature.

At temperature T, the ratio between $N_e(T)$ (the number of electrons) and $N_{\rm P}(T)$ (the number of polarons) is given by[25]

$$[\frac{N_e(T)}{N_{\rm P}(T)}]^2 = e^{2\frac{\Delta f(T)}{k_B T}}, \tag{11}$$

where we assume that the formation free energy of hole polarons is the same as that of electron polarons. We can see from Fig.1(b) that the below 140 K, the number of electrons is negligible. At 300 K, $N_e(T)/N_{\rm P}(T) \sim 0.1$. Therefore, the dominant carriers in $MAPbI_3$ are large polarons, as opposed to electrons and holes.

III. DIELECTRIC SCREENING

There is a misconception in literature which attributes the temperature dependence of carrier mobility, i.e., $\mu \propto T^{-3/2}$ entirely to the scattering of acoustic phonons. This misconception counters the fact that many non-polar semiconductors do not exhibit the same $T^{-3/2}$ dependence as the perovskite materials although their carriers are scattered primarily by acoustic phonons[28]. We believe that the perovskites possess a unique but often overlooked feature, i.e., the existence of a spontaneously polarized phase at low temperatures, which is responsible for the unique temperature dependence of carrier mobility. More specifically, we will reveal in following that it is the temperature dependence of the dielectric function that among other factors, yields the temperature dependence of carrier mobility in the perovskites.

Recent molecular dynamics simulations indicate that there exists a super paraelectric phase in $MAPbI_3$ below 1000K [20]. It is known that the super paraelectric phase emerges from a spontaneously polarized phase with increased temperature. For ABX_3 perovskites, the critical polarizability α_c above which a spontaneous polarization takes place is given by $\alpha_c = (a/2)^3/0.383$ [29]. For $MAPbI_3$, $\alpha_c = 8.16 \times 10^{-29}$ m^3. On the other hand, the polarizability of $MAPbI_3$, $\alpha_{\rm dis}$ is mainly induced by the displacements of Pb^{2+} and I^- ions and can be estimated as $\alpha_{\rm dis} = 2.73 \times 10^{-28}{\rm m}^3 > \alpha_c$ [30]. Hence, below a certain temperature, $MAPbI_3$ is spontaneously polarized.

For a super paraelectric phase, one can express its dielectric function as follows:[29,31–33]

$$\varepsilon(\omega, T) = \varepsilon_\infty + \frac{1}{3}\frac{n_d p^2}{k_B T \epsilon_0}\frac{1}{1 - i\omega\tau(T)} \tag{12}$$

$$+\frac{9}{\beta(T-\theta)}\frac{\omega_{ip}^2}{\omega'^2 - i\gamma'\omega - \omega^2}.$$

The first term represents the contribution from the bound electrons at the optical frequencies and room temperature and it is taken from an experimental measurement ($\varepsilon_\infty \approx 6.5$)[18]. The second term stems from the rotations of MA ions. The dipole moment of the MA cation is $p = 7.64 \times 10^{-30}$C·m and the number density of the cations is $n_d \approx 4 \times 10^{27}{\rm m}^{-3}$ [34]. $\tau(T)$ is the temperature dependent relaxation time of the MA ions[32] which is about 0.2 -14 ps[32,35,36]. The third term represents the contribution of the displacements of Pb^{2+} and I^- ions, and the factor $9/\beta(T-\theta)$ account for the static susceptibility[29,37]. ω_{ip} is the frequency of ionic plasmon; ω' and γ' are the eigenfrequency and friction coefficient of the Pb-I stretching mode[31]. β is a constant[29] with a dimension of inverse temperature (K^{-1}). It turns out that in $MAPbI_3$, $\theta \sim 0$K is a small number[30] compared to T. If the spontaneously polarized phase below the critical temperature is ferroelectric, $\theta > 0$. If the phase is anti-ferroelectric, $\theta < 0$ [33].

If the frequency ω is so low ($\omega \ll 7 \times 10^{10}$Rad/s) that the product $\omega\tau(T) \ll 1$, $[1 - i\omega\tau(T)]^{-1} \sim 1$. Hence the second term reduces to $n_d p^2/(3k_B T\epsilon_0)$. Specifically, at T = 300K and $\omega = 0$, the second terms becomes a constant (2). Therefore, the second term and the third term scale approximately as $1/T$, and Eq.(12) becomes

$$\varepsilon(\omega, T) = \varepsilon_\infty + C(\omega)/T, \tag{13}$$

where $C(\omega)$ is a materials constant, independent of temperature. This result agree very well with the experimental data at $\omega/2\pi = 1$KHz above 160K (cf. Fig. 3 of [19]) as shown in Fig. 2. Note that this $1/T$ dependence is analogous to Curie-Weiss law due to magnetic phase transitions.

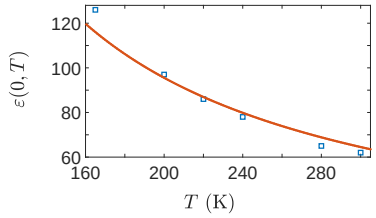

FIG. 2. Static dielectric constant as function of temperature in $MAPbI_3$. The experimental data (squares) are taken from [19], and the solid line is a fit from Eq. (13).

If ω is $7 \times 10^{10} - 10^{12}$Rad/s, $\omega\tau(T) \sim 1$. In this frequency range, the second term becomes a dominant

contribution. As a result, $\varepsilon(\omega, T)$ deviates from the $1/T$ behavior, as found experimentally in the case of $\omega/2\pi =$ 90GHz in [32].

As will be shown later, the screened polaron-LA phonon interaction is responsible for charge transport in the perovskites. The characteristic acoustic phonon frequency is $\omega_b = c_l\pi/a$, where a is the lattice constant and c_l is the speed of longitudinal sound wave. In $MAPbI_3$, $\omega_b \sim 10^{13}$Rad/s [30]. For such a high frequency, $\omega\tau(T) \gg 1$, the second term can be ignored, and Eq.(12) is reduced to Eq.(13) again.

It is experimentally observed that below 150 -160 K, $\varepsilon(\omega, T)$ deviates from the $1/T$ behavior[19], giving rise to contrasting transport behaviors[9]. This deviation is caused by structural phase transition from tetragonal to orthorhombic phase.

IV. CHARGE TRANSPORT AND CARRIER MOBILITY

A. Polaron-LA phonon vs. polaron-LO phonon interaction

It is generally accepted that as quasiparticles, large polarons result from the interaction between electrons (or holes) with optical phonons in ionic perovskites[10,11,13,20,22]. However, it is often mistakenly assumed that the same optical phonons must also be principally responsible for scatting of the large polarons. This assumption would yield incorrect temperature dependence of carrier mobility, which is the source of confusion and debate in literature[10–13]. Here we demonstrate that much of the electron-LO phonon interaction $h_{\text{e-LO}}$ is involved in the formation of large polarons, thus the residual interaction $h_{\text{P-LO}}$ is substantially weaker than the interaction between the polaron and the LA phonon, $h_{\text{P-Aph}}$ in $MAPbI_3$. Based on Born-Huang model of electron-optical phonon interaction, we can show

$$h_{\text{e-LO}}/h_{\text{e-LA}} \sim \frac{\frac{3}{2}\hbar\omega_{\text{LO}}(\frac{\hbar}{2m\omega_{\text{LO}}})^{1/4}[4\pi\alpha]^{1/2}}{\frac{1}{\varepsilon}\sqrt{\frac{\hbar}{2M_j c_l k_b}}2\frac{e^2}{\epsilon_0}n_{\text{cell}}^{1/2}}. \quad (14)$$

Here n_{cell} is the number of primitive unit cells in a unit volume. One can see that a softer lattice (smaller sound speed c_l), larger primitive unit cell (smaller k_b and n_{cell}) and smaller ω_{LO} will increase the relative importance of $h_{\text{e-LA}}$. Since the electronic part of the polaron wave-function is similar to the free electron wave-function, $h_{\text{P-LA}} \approx h_{\text{e-LA}}$. On the other hand, according to the Feynman model of large polarons,

$$h_{\text{P-LO}} \sim (\alpha/10)^4 h_{\text{e-LO}}, \quad (15)$$

where α is a dimensionless coupling constant[38]. Combining Eq.(14) to Eq.(15), one has

$$\frac{h_{\text{P-LO}}}{h_{\text{P-LA}}} \sim (\alpha/10)^4 \frac{\frac{3}{2}\hbar\omega_{\text{LO}}(\frac{\hbar}{2m\omega_{\text{LO}}})^{1/4}[4\pi\alpha]^{1/2}}{\frac{1}{\varepsilon}\sqrt{\frac{\hbar}{2M_j c_l k_b}}2\frac{e^2}{\epsilon_0}n_{\text{cell}}^{1/2}}. \quad (16)$$

With the material parameters for $MAPbI_3$, we find $h_{\text{P-LO}}/h_{\text{P-LA}} \sim 0.12$. This result is supported by the experiments which reported[12,39] $h_{\text{P-LO}}/h_{\text{P-LA}} \sim 0.1$. Therefore, the acoustic phonons are chiefly responsible for the scattering while the optical phonons are responsible for the formation of the large polarons in $MAPbI_3$. Recent experiments also suggest that the e-LO phonon interaction is primarily responsible for the line-width of photoluminescence (PL) spectrum of the perovskites[12], which is consistent with the preceding analysis. As mentioned earlier, since electrons and holes are stabilized by the interaction with the optical phonons, they have to be "activated" prior to recombination, by absorbing optical phonons. After the annihilation, the optical phonons have to be emitted to restore the deformed lattice. The energy of the absorbed and emitted phonons is responsible for the PL line-width.

B. Scattering mechanisms

The Hamiltonian of the system can be written as

$$H = K_{\text{P}} + H_{\text{PP}} + H_{\text{P-def}} + H_{\text{P-LA}} + H_{\text{LA}}, \quad (17)$$

where K_{P} denotes the sum of single polaron Hamiltonians, and H_{PP} is the Coulomb interaction between the polarons. $H_{\text{P-def}}$ represents the interaction between the polarons and defects whereas $H_{\text{P-LA}}$ is the interaction between the polarons and longitudinal acoustic (LA) phonons; H_{LA} is the Hamiltonian of LA phonons. The interaction between the polarons and transverse phonons, and the residual interaction between the polarons and LO phonons are small, and can be neglected. Note that H_{PP}, $H_{\text{P-def}}$ and $H_{\text{P-LA}}$ represent dressed or effective interactions and are related to the corresponding bare interactions via the dielectric function, e.g., $H_{\text{PP}} = H_{\text{PP}}^{\text{bare}}/\varepsilon(\omega, T)$.

We next apply the Boltzmann equation to elucidate the transport behavior of large polarons in the perovskites. The key physical quantity of interest is distribution function of the polarons, whose temporal rate change is given by total collision frequency ν_t, including scattering contributions of polaron-polaron, polaron-defect and polaron-LA phonon. ν_t is related to the charge carrier mobility μ by $\mu = e/m_{\text{P}}\nu_t$. We show that the large polarons are stable against the three collision processes in Supporting Information and to a good approximation, we can describe the translational motion of the polarons by plane-waves. Thus the energy of the polaron is given as $\varepsilon_{\mathbf{p}} = \mathbf{p}^2/2m_{\text{P}}$, where $\mathbf{p}$ is the plane-wave momentum. We denote the non-equilibrium distribution function of polarons in state $|\mathbf{p}\rangle$ as $f_{\mathbf{p}}(t)$, and the distribution function of the LA phonons as $N_{\mathbf{k}}(t)$ ($\mathbf{k}$ is the wave vector of the phonons) and their corresponding equilibrium counterparts are given as f_0 and N_0.

The change rate of $f_{\mathbf{p}}(t)$ due to the polaron and LA phonon collision is given by $\nu_{\text{P-LA}} = (\partial f_{\mathbf{p}}/\partial t)_{\text{P-LA}}$ and is

calculated in the following.

$$(\frac{\partial f_{\mathbf{p}}}{\partial t})_{\text{P-LA}} = -\sum_{\mathbf{k}} \frac{\partial N_0(\omega_{\mathbf{k}})}{\partial \hbar\omega_{\mathbf{k}}}[f_0(\mathbf{p}') - f_0(\mathbf{p})] \tag{18}$$

$$\{w(\mathbf{p}', \mathbf{k}; \mathbf{p})(\varphi_{\mathbf{p}'} - \varphi_{\mathbf{p}} + \chi_{\mathbf{k}})\delta(\varepsilon_{\mathbf{p}} - \varepsilon_{\mathbf{p}'} - \hbar\omega_{\mathbf{k}})$$

$$-w(\mathbf{p}'; \mathbf{p}, \mathbf{k})(\varphi_{\mathbf{p}'} - \varphi_{\mathbf{p}} - \chi_{\mathbf{k}})\delta(\varepsilon_{\mathbf{p}} - \varepsilon_{\mathbf{p}'} + \hbar\omega_{\mathbf{k}})\}.$$

Here φ and χ describe the deviations of $f_{\mathbf{p}}$ and $N_{\mathbf{k}}$ from their equilibrium values: $f_{\mathbf{p}} - f_0(\varepsilon) = -\varphi\partial f_0(\varepsilon)/\partial\varepsilon$, and $N_{\mathbf{k}} - N_0(\mathbf{k}) = -\chi\partial N_0(\omega_{\mathbf{k}})/\partial\hbar\omega_{\mathbf{k}}$. $w(\mathbf{p}', \mathbf{k}; \mathbf{p})$ is the probability amplitude defined as $w(\mathbf{p}', \mathbf{k}; \mathbf{p})(N_{\mathbf{k}} + 1) = 2\pi|\langle\mathbf{p}', \mathbf{k}|H_{\text{P-LA}}(\text{emission})|\mathbf{p}\rangle|^2/\hbar$, $w(\mathbf{p}'; \mathbf{p}, \mathbf{k})$ is defined by $w(\mathbf{p}'; \mathbf{p}, \mathbf{k})N_{\mathbf{k}} = 2\pi|\langle\mathbf{p}'|H_{\text{P-LA}}(\text{absorption})|\mathbf{p}, \mathbf{k}\rangle|^2/\hbar$ [40]. Similar rate equations can be obtained for $\nu_{\text{P-def}}$ and ν_{PP} and their expressions are given in Supporting Information.

The characteristic frequency of the LA phonons is $\omega_b = c_s k_b$, where c_s is the average sound speed in the longitudinal direction. $k_b = \pi/a$ is the wave-vector at the Brillouin zone boundary[14]. Because the elastic constants of the perovskites are relatively small, c_s and ω_b are also small. In the tetragonal phase[41,42] of $MAPbI_3$, $c_s \approx 2147$ m/s, and $\omega_b \sim 82$ K. In the pseudo-cubic phase[41,42], $c_s \approx 2824$ m/s, $\omega_b \sim 107$ K. Thus at room temperature, $k_B T \gtrsim \hbar\omega_b$ and the LA phonons are fully excited[9]. These fully excited LA phonons increase the P-LA scattering probability and are principally responsible for polaron scattering. In addition, the phonon distribution function $N_0(\omega_{\mathbf{k}})$ in Eq. (18) can be reduced to $N_0(\omega_{\mathbf{k}}) \approx k_B T/\hbar\omega_{\mathbf{k}}$.

We can now derive an analytical expression for the change rates $\partial f_{\mathbf{p}}/\partial t$ induced by the three collision processes H_{PP}, $H_{\text{P-def}}$ and $H_{\text{P-LA}}$. More specifically, change rate due to the polaron-polaron scattering is given by[30,43] $\nu_{\text{PP}} = (\partial f_{\mathbf{p}}/\partial t)_{\text{PP}}$:

$$\nu_{\text{PP}} \sim \left[\frac{T}{300\varepsilon_{s1} + (T - 300)\varepsilon_\infty}\right]^2 n \tag{19}$$

$$\frac{4\pi^{3/2}\hbar^3 e^{-3/2}}{(2m_{\text{P}}k_B T)^{3/2}}\frac{1}{\hbar}\frac{d^4}{a^6}(\frac{e^2}{\epsilon_0})^2\frac{(kT)^2}{D^3},$$

where the dielectric function $\varepsilon_{s1} = \varepsilon(\omega_b, 300)$; $D \sim 3$ eV is the conduction band width[21,22,44] of $MAPbI_3$ and $d = 2R_{\text{P}}$ is the diameter of the polaron. The change rate due to the polaron-defect scattering is[14,30,40] given by $\nu_{\text{P-def}} = (\partial f_{\mathbf{p}}/\partial t)_{\text{P-def}}$:

$$\nu_{\text{P-def}} \sim \left[\frac{T}{300\varepsilon_{s1} + (T - 300)\varepsilon_\infty}\right]^2 C\frac{2\pi}{\hbar} \tag{20}$$

$$\left(\frac{e^2\Delta z}{\epsilon_0}\right)^2 \frac{1}{D^2 a^3}\frac{\hbar^4}{(2m_{\text{P}}k_B T)^2}k_B T,$$

where C is the number of defects per cubic meter and Δz is the effective charge of the defect. The change rate due to polaron and LA phonon scattering is given by $\nu_{\text{P-LA}} = (\partial f_{\mathbf{p}}/\partial t)_{\text{P-LA}}$:

$$\nu_{\text{P-LA}} \sim \left[\frac{T}{300\varepsilon_{s1} + (T - 300)\varepsilon_\infty}\right]^2 \frac{\pi}{M\omega_b k_b^2 a^3}$$

$$\frac{4\pi}{3}k_b^3(\frac{ze^2}{\epsilon_0})^2(\frac{k_B T}{\hbar\omega_b})^2 n\frac{4\pi^{3/2}\hbar^3 e^{-3/2}}{(2m_{\text{P}})^{3/2}(k_B T)^{5/2}}, \tag{21}$$

where z is the weighted nuclear charges of the ions and M is the reduced mass of Pb and I ions.

It is known that dominant defects in halide perovskites are not particularly harmful to charge transport because they do not create detrimental deep levels within the band gap[45–47]. Therefore, in our model, only shallow defects are considered, which could induce lattice deformation and charge states at the defect center. Because polaron scattering due to the former is much smaller than the latter, we can approximate $H_{\text{P-def}}$ by Coulomb interaction between the point charges at the defect center and the polarons.

To compare the relative importance of the scattering processes, we evaluate the three terms by taking I^- vacancies as an example of defects in $MAPbI_3$. We assume a moderate defect concentration at $C = 4.0 \times 10^{20}\text{cm}^{-3}$ and $\Delta z = 1.22$. The consideration of other point defects will only change Δz by a small amount (Δz = 1 - 3). The three contributions as a function of temperature are plotted in Fig. 3. We find that at room temperature $\nu_{\text{P-Aph}} \gg \nu_{\text{P-def}} \gg \nu_{\text{PP}}$. Therefore, the polaron-LA phonon scattering dominates charge transport in $MAPbI_3$, and μ would appear insensitive to the defects.

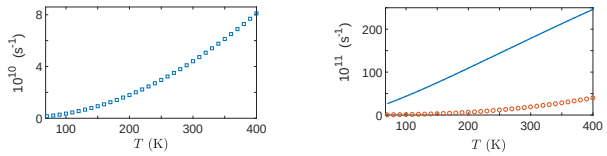

(a) (b)

FIG. 3. (a) The polaron-polaron collision frequency as a function of T determined by Eq.(19); (b) The polaron-I^- vacancy collision frequency (circles) and the polaron-LA phonon collision frequency (solid line) as functions of T determined by Eq. (20) and (21). $\varepsilon_0 = 70$ and $\varepsilon_\infty = 6.5$ [18] are used in the plot.

C. Concentration dependence of mobility

If we ignore $\nu_{\text{P-def}}$ and ν_{PP}, we arrive at the key result of the model:

$$\mu \propto n^{-1} m_{\text{P}}^{1/2} T^{-3/2}. \tag{22}$$

First, we find that the mobility is inversely proportional to the carrier concentration n, and this finding is consistent to the experimental measurements[4] in p-doped $MAPbI_3$. In Fig. 4(a), we compare the experimental hole mobility μ_h (squares) with the theoretical values (solid line) as a function of n^{-1} where a good agreement is found.

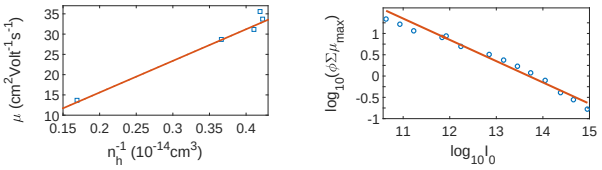

(a) (b)

FIG. 4. (a) Hole mobility μ vs. n_h^{-1} for p-doped $MAPbI_3$. The experimental data (squares) are taken from [4]; the solid line is a fit of Eq. (22). (b) The logarithm of the effective carrier mobility, $\log_{10}\phi\Sigma\mu$ is plotted as a function of the logarithm of incident photon flux, $\log_{10} I_0$. The experimental data (circles) are taken from [5], and the solid line is a fit of Eq. (23).

Let γ be the electron-hole recombination coefficient, κ the generation probability per impinging photon and G the volume density of photons in the sample, we can express $n = (\gamma^{-1}\kappa G)^{1/2}$ by assuming n is much larger than the trap center concentration. Here, $G = I_0/l_{\rm abs}$, I_0 is the incident photon flux and $l_{\rm abs}$ is the absorption length[26]. Substitute the expression of n into Eq. (22), one obtains:

$$\mu \propto (l_{\rm abs}\gamma)^{1/2}(\kappa I_0)^{-1/2}T^{-3/2}. \qquad (23)$$

The circles in Fig. 4(b) are experimental data[5] for effective mobility $\phi\mu$ vs. incident flux I_0, and the solid line is a fit based on Eq. (23). Here we have to adjust the intercept due to a lack of experimental values of κ, $l_{\rm abs}$ and γ in [5], nevertheless the agreement in the slope between the theory and the experiment is very good.

D. Temperature dependence of mobility

Finally, we compare the theoretical prediction with experimental data on carrier mobility as a function of temperature making use of Eq. (21) and $\mu(T) = e/m_{\rm P}\nu_{\text{P-LA}}$. Because the values of ε_0, ε_∞ and n are not available in the experiments[6,7], we have to use n as a fitting parameter in the comparison. By taking $\varepsilon_\infty = 4.5$ and $\varepsilon_0 = 24.5$ from first-principles calculations[20,21], we can fit the theoretical mobility to the experimental data in Fig. 5. For the first experiment[6], $n = 2.3\times10^{17}\text{cm}^{-1}$ was used in the fitting while for the second experiment[7], $n = 8.3\times10^{17}\text{cm}^{-1}$ was used in the fitting. Both values of n are reasonable[26] and for both cases, satisfactory agreements to the experimental data are obtained.

In a recent experiment by Hutter et al., the temperature dependence of carrier mobility in $MAPbI_3$ was

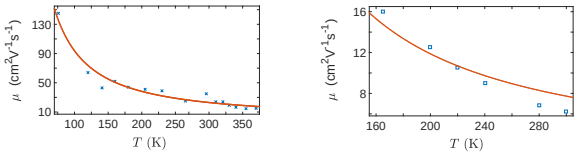

(a) (b)

FIG. 5. The carrier mobility μ as a function of temperature. The solid curves are obtained from Eq. (21) with fitting a parameter of n. (a) The experimental data (crosses) is from [6], and $n = 2.3\times10^{17}\text{cm}^{-3}$. (b) The experimental data (squares) is from 7, and $n = 8.3\times10^{17}\text{cm}^{-3}$.

shown to exhibit two regimes of contrasting behaviors[9]. Above 150 K, carrier mobility $\mu(T) \propto T^{-3/2}$ while below 150 K, the mobility drops precipitately, decreasing with decreased temperature. Using the experimental dielectric function $\varepsilon(\omega, T)$ for $\omega/2\pi$ = 1KHz as obtained in[19], our analytical expression in Eq. (21) can reproduce the experimental data of Hutter reasonably well in both regimes, as shown in Fig.6. In the tetragonal phase ($T > 150$ K), the mobility behaves as $\mu(T) \propto T^{-3/2}$, while in the orthorhombic phase ($T < 150$K), the mobility decreases with decreasing temperature with a sharp drop around 150 K. We further speculate that the reason that the earlier experiments observed only the regime of $\mu(T) \propto T^{-3/2}$ is due to the presence[9,48] of the tetragonal phase at $T < 150$ K.

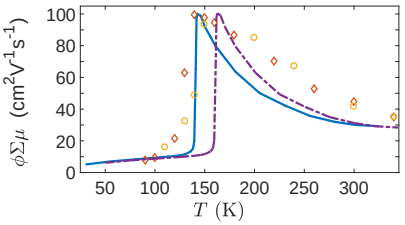

FIG. 6. Product of generation yield ϕ and mobility $\Sigma\mu$ as function of temperature. Circles (diamonds) are measured during the heating (cooling) process [9]. The dash line is calculated from the experimental dielectric function [19] and the solid line is obtained by shifting the the tetragonal-orthorhombic transition temperature from [19] to [9].

V. SUMMARY

In conclusion, we proposed a theoretical model that can elucidate key experimental observations on charge transport in hybrid perovskite materials. Essential to the model is improved understanding crucial to charge transport, including that the acoustic phonons as opposed to the optical phonons are responsible for the scattering of large polarons, the acoustic phonons are fully excited due to the "softness"of the perovskites, and the temperature dependent dielectric function is the key contributor to the temperature dependence of the mobility. Analytic

expressions were given for various contributions to the carrier mobility and compared to the experimental measurements with good agreements. By directly relating the carrier mobility to material parameters, the present work may provide guidance for materials design and form a starting point for more rigorous first-principles predictions of transport properties.

The work at California State University Northridge was supported by NSF-PREM program via grant DMR-1205734. Discussion with Guangjun Nan is acknowledged. The authors wish to thank anonymous referees for their stimulating comments.
†haiqing0@csrc.ac.cn, *ganglu@csun.edu

[1] G. Grancini, A. R. S. Kandada, J. M. Frost, A. J. Barker, M. D. Bastiani, M. Gandini, S. Marras, G. Lanzani, A. Walsh, and A. Petrozza, Nature Photonics **9**, 695701 (2015).

[2] Q. Dong, Y. Fang, Y. Shao, P. Mulligan, J. Qiu, L. Cao, and J. Huang, Science **347**, 967 (2015).

[3] M. I. Saidaminov, A. L. Abdelhady, B. Murali, E. Alarousu, V. M. Burlakov, W. Peng, I. Dursun, L. Wang, Y. He, G. Maculan, A. Goriely, T. Wu, O. F. Mohammed, and O. M. Bakr, Nature Communications **6**, 7586 (2015).

[4] C. Bi, Y. Shao, Y. Yuan, Z. Xiao, C. Wang, Y. Gao, and J. Huang, J. Mater. Chem. A **2**, 18508 (2014).

[5] H. Oga, A. Saeki, Y. Ogomi, S. Hayase, and S. Seki, Journal of the American Chemical Society **136**, 13818 (2014).

[6] R. L. Milot, G. E. Eperon, H. J. Snaith, M. B. Johnston, and L. M. Herz, Advanced Functional Materials **25**, 6218 (2015).

[7] T. J. Savenije, C. S. Ponseca, L. Kunneman, M. Abdellah, K. Zheng, Y. Tian, Q. Zhu, S. E. Canton, I. G. Scheblykin, T. Pullerits, A. Yartsev, and V. Sundstrm, The Journal of Physical Chemistry Letters **5**, 2189 (2014).

[8] M. Karakus, S. A. Jensen, F. DAngelo, D. Turchinovich, M. Bonn, and E. Cnovas, The Journal of Physical Chemistry Letters **6**, 4991 (2015).

[9] E. M. Hutter, M. C. Gelvez-Rueda, A. Osherov, V. Bulovic, F. C. Grozema, S. D. Stranks, and T. J. Savenije, Nat Mater **16**, 115 (2017).

[10] X.-Y. Zhu and V. Podzorov, The Journal of Physical Chemistry Letters **6**, 4758 (2015).

[11] T. M. Brenner, D. A. Egger, A. M. Rappe, L. Kronik, G. Hodes, and D. Cahen, The Journal of Physical Chemistry Letters **6**, 4754 (2015).

[12] A. D. Wright, C. Verdi, R. L. Milot, G. E. Eperon, M. A. Perez-Osorio, H. J. Snaith, F. Giustino, M. B. Johnston1, and L. M. Herz, Nature Communications **7**, 11755 (2016).

[13] M. Sendner, P. K. Nayak, D. A. Egger, S. Beck, C. Muller, B. Epding, W. Kowalsky, L. Kronik, H. J. Snaith, A. Pucci, and R. Lovrincic, Mater. Horiz. **3**, 613 (2016).

[14] J. Callaway, *Quantum Theory of the Solid State*, 2nd ed. (Academic Press, 2013).

[15] D. Emin, *Polarons* (Cambridge University Press, 2013).

[16] EnvironmentalChemistry.com, `http://environmentalchemistry.com/yogi/periodic/ionicradius.html` (2016).

[17] Wikipedia, `https://en.wikipedia.org/wiki/Ionic_radius` (2016).

[18] Q. Lin, A. Armin, R. C. R. Nagiri, P. L. Burn, and P. Meredith, Nat Photon **9**, 106 (2015).

[19] N. Onoda-Yamamuro, T. Matsuo, and H. Suga, Journal of Physics and Chemistry of Solids **53**, 935 (1992).

[20] J. M. Frost, K. T. Butler, and A. Walsh, APL Materials **2**, 081506 (2014).

[21] F. Brivio, K. T. Butler, A. Walsh, and M. van Schilfgaarde, Phys. Rev. B **89**, 155204 (2014).

[22] E. Menendez-Proupin, P. Palacios, P. Wahnon, and J. C. Conesa, Physical Review B **90**, 045207 (2014).

[23] M. Bokdam, T. Sander, A. Stroppa, S. Picozzi, D. D. Sarma, C. Franchini, and G. Kresse, Scientific Reports **6**, 28618 (2016).

[24] J. M. Frost, arXiv.org (2017), arXiv:1704.05404v3 [cond-mat.trl-sci].

[25] L. D. Landau and E. M. Lifshitz, *Statistical Physics, Part 1*, 3rd ed. (Butterworth-Heinemann, 1980).

[26] Y. Chen, H. T. Yi, X. Wu, R. Haroldson, Y. N. Gartstein, Y. I. Rodionov, K. S. Tikhonov, A. Zakhidov, X. Y. Zhu, and V. Podzorov, Nature Communications **7**, 12253 (2016).

[27] T. L. Hill, *An Introduction to Statistical Thermodynamics* (Dover Publications, 1987).

[28] B. V. Zeghbroeck, "Principles of semiconductor devices," `http://ecee.colorado.edu/~bart/book/book/chapter2/ch2_7.htm` (2011).

[29] R. P. Feynman, R. B. Leighton, and M. Sands, *The Feynman Lectures on Physics*, Vol. 2 (Addison-Wesley, 1977).

[30] Supplemental Material `http://link.aps.org/supplemental/` (2017).

[31] J. Schwinger, L. L. Deraad Jr., K. A. Milton, W.-Y. Tsai, and J. Norton, *Classical Electrodynamics* (Westview Press, 1998).

[32] A. Poglitsch and D. Weber, The Journal of Chemical Physics **87**, 6373 (1987).

[33] C. Kittel, *Solid State Physics*, 5th ed. (John Wiley, 1976).

[34] J. M. Frost, K. T. Butler, F. Brivio, C. H. Hendon, M. van Schilfgaarde, and A. Walsh, Nano Letters **14**, 2584 (2014).

[35] A. M. A. Leguy, J. M. Frost, A. P. McMahon, V. G. Sakai, W. Kockelmann, C. Law, X. Li, F. Foglia, A. Walsh, B. C. ORegan, J. Nelson, J. T. Cabral, and P. R. F. Barnes, Nature Communications **6**, 7124 (2015).

[36] R. E. Wasylishen, O. Knop, and J. B. Macdonald, Solid State Communications **56**, 581 (1985).

[37] C. Kittel, *Quantum Theory of Solids*, 2nd ed. (Wiley, 1987).

[38] R. P. Feynman, Phys. Rev. **97**, 660 (1955).

[39] E. Menndez-Proupin, C. L. Beltrn Ros, and P. Wahnn, Physica Status Solidi (RRL) Rapid Research Letters **9**, 559 (2015).

[40] E. M. Lifshitz and L. P. Pitaevskii, *Physical Kinetics*, 1st ed. (Butterworth-Heinemann, 1981).

[41] Y. He and G. Galli, Chemistry of Materials **26**, 5394 (2014).

[42] X. Qian, X. Gu, and R. Yang, Applied Physics Letters **108**, 063902 (2016).

[43] R. E. Peierls, *Quantum Theory of Solids* (Oxford University Press, 2001).

[44] P. Umari, E. Mosconi, and F. D. Angelis, Scientific Reports **4**, 4467 (2014).
[45] W.-J. Yin, J.-H. Yang, J. Kang, Y. Yan, and S.-H. Wei, J. Mater. Chem. A **3**, 8926 (2015).
[46] W.-J. Yin, T. Shi, and Y. Yan, Applied Physics Letters **104**, 063903 (2014).
[47] J. L. Miller, Physics Today **67**, 11 (2014).
[48] W. Kong, Z. Ye, Z. Qi, B. Zhang, M. Wang, A. Rahimi-Iman, and H. Wu, Phys. Chem. Chem. Phys. **17**, 16405 (2015).